Geophys. J. Int. (2010) **181,** 521–531 doi: 10.1111/j.1365-246X.2010.04519.x

Seismic reflectivity of the sediment-covered seafloor: effects of velocity gradients and fine-scale layering

Rolf Sidler and Klaus Holliger

Institute of Geophysics, University of Lausanne, CH-1015 *Lausanne, Switzerland. E-mail: rsidler@gmail.com*

Accepted 2010 January 8. Received 2010 January 7; in original form 2009 June 19

SUMMARY

Knowledge of the reflectivity of the sediment-covered seabed is of significant importance to marine seismic data acquisition and interpretation as it governs the generation of reverberations in the water layer. In this context pertinent, but largely unresolved, questions concern the importance of the typically very prominent vertical seismic velocity gradients as well as the potential presence and magnitude of anisotropy in soft surficial seabed sediments. To address these issues, we explore the seismic properties of granulometric end-member-type clastic sedimentary seabed models consisting of sand, silt, and clay as well as scale-invariant stochastic layer sequences of these components characterized by realistic vertical gradients of the *P*- and *S*-wave velocities. Using effective media theory, we then assess the nature and magnitude of seismic anisotropy associated with these models. Our results indicate that anisotropy is rather benign for *P*-waves, and that the *S*-wave velocities in the axial directions differ only slightly. Because of the very high *P*- to *S*-wave velocity ratios in the vicinity of the seabed our models nevertheless suggest that *S*-wave triplications may occur at very small incidence angles. To numerically evaluate the *P*-wave reflection coefficient of our seabed models, we apply a frequency-slowness technique to the corresponding synthetic seismic wavefields. Comparison with analytical plane-wave reflection coefficients calculated for corresponding isotropic elastic half-space models shows that the differences tend to be most pronounced in the vicinity of the elastic equivalent of the critical angle as well as in the post-critical range. We also find that the presence of intrinsic anisotropy in the clay component of our layered models tends to dramatically reduce the overall magnitude of the *P*-wave reflection coefficient as well as its variation with incidence angle.

Key words: Numerical solutions; Fractals and multifractals; Seismic anisotropy; Seismic attenuation; Wave propagation; Acoustic properties.

1 INTRODUCTION

The *P*-wave reflection coefficient of the seafloor is an important parameter for the acquisition, processing and interpretation of marine seismic data in general and of multicomponent ocean bottom seismic recordings in particular (e.g. Schneider & Backus 1964; Amundsen & Reitan 1995; Sheriff & Geldart 1995; Caldwell 1999; Stewart *et al.* 2002, 2003; Wang *et al.* 2002; Schalkwijk *et al.* 2003; Muijs *et al.* 2004; Edme *et al.* 2005; Muijs *et al.* 2007; Edme & Singh 2008, 2009). To date, essentially all corresponding seafloor models have been based on the assumption of a homogeneous, elastic and isotropic half-space overlain by a homogeneous acoustic water layer. Although the assumptions for the water layer are likely to be a reasonably adequate approximation of the physical reality, this is not the case for the surficial seabed, which in general is covered by soft, unconsolidated sediments characterized by strong seismic velocity–depth gradients as well as pronounced attenuation (Hamilton 1972; Carlson *et al.* 1984; Berge *et al.* 1991). Moreover, at least in certain geological environments, the surficial sedimentary cover of the seabed must be expected to be seismically anisotropic (Banik 1984; Hornby *et al.* 1994; Vernik & Liu 1997).

The effects of attenuation in the surficial seabed have recently been investigated by Carcione & Helle (2004) and Eggenberger *et al.* (2005). The results of these studies indicate that the presence of attenuation significantly affects the amplitude-versus-offset (AVO) behaviour of seismic reflections from the seabed with regard to a corresponding elastic equivalent and thus may lead to erroneous estimates of the seismic material parameters in general and of the *S*-wave velocity in particular. Conversely, the corresponding effects of strong vertical velocity gradients as well as the nature, magnitude and implications of seismic anisotropy in the sediment-covered seabed on its reflection coefficient are largely unexplored. The primary reasons for this are (1) that the strong vertical velocity gradients are not amenable to analytical solutions and are very hard to adequately parameterize and accommodate for corresponding numerical approaches and (2) that the presence of anisotropy in soft surficial seabed sediments is

very difficult to observe and quantify both in the field and in the laboratory.

The purpose of this paper therefore is to alleviate these problems and to numerically evaluate seismic reflection coefficients for the sediment-covered seabed for a range of pertinent and realistic models. In particular, we seek to constrain the magnitude and nature of the anisotropy that could potentially be present in surficial unconsolidated seabed sediments and to explore its effects in conjunction with realistic velocity–depth gradients. In doing so, we focus on clastic sediments prevailing throughout the oceanic shelf and continental slope regions, which are important to seismic exploration. Although there is a significant body of literature on seismic velocity and attenuation measurements in the shallow seabed (Hamilton 1972, 1976, 1979, 1980; Bryan & Stoll 1988; Stoll 1989; Bowles 1997; Buckingham 2005; Jackson & Richardson 2007), observations regarding the presence and importance of seismic anisotropy in surficial marine sediments are few and far between (Bachman 1979, 1983; Carlson *et al.* 1984; Berge *et al.* 1991; Odom *et al.* 1996). Although little is known regarding the nature and origin of seismic anisotropy in unconsolidated seabed sediments, the most likely causes are intrinsic anisotropy due to the mineralogical constituents (Vega-Ruiz 2003) as well as fine-scale layering (Postma 1955; Carlson *et al.* 1984).

The paper proceeds as follows: To obtain order-of-magnitude-type estimates of anisotropy and its variability, we develop a conceptual seismic model of the sediment-covered seafloor based on end-member-type clastic sedimentary deposits as well as on realistic scale-invariant stochastic layer sequences of these components in conjunction with pertinent velocity–depth gradients. We then explore the implications for seismic wave propagation through effective media theory and numerical evaluations of the reflection coefficients of these seabed models and compare the results with those obtained for the corresponding homogeneous, isotropic equivalents.

2 VELOCITY MODELS

2.1 Large-scale bulk properties

Our first objective is to use the available literature to define representative 1-D models of the seismic velocity distribution for a surficial seabed covered with unconsolidated clastic sediments. In doing so, we follow the common practice in ocean acoustics to describe clastic seabed sediments based on their granulometric characteristics (e.g. Bowles 1997; Jackson & Richardson 2007). The end-member sediments resulting from this approach are sand, silt and clay (Shepard 1954), which are indeed the dominant individual components in typical clastic marine sediments. Bowles (1997) presents a comprehensive review of the literature available on the seismic parameters of surficial seabed sediments. The seismic velocity–depth distribution of sandy seabeds seems to be most adequately characterized through the relationships put forward by Hamilton (1979) and Hamilton (1987) (Table 1). These equations have also been used by Buckingham (2005) for comparison with his theoretical geo-acoustical model, which is based on an unconsolidated granular medium with the grains in mutual contact but not welded together. For our intents and purposes, the two other end-member-type sediments are silt and clay, which tend to have sufficiently similar bulk seismic properties to be lumped into one single group (Bowles 1997). The corresponding *P*-wave velocity model is based on the work of Hamilton (1980). The results obtained using the corresponding linear equation in Table 1 agree well with recent laboratory measurements from Mondol *et al.* (2007). The *S*-wave velocity model for silty/clayey seabeds is adopted from Lovell & Odgen (1984).

In view of the inconsistency and uncertainty of the available data regarding the dissipative properties of surficial marine sediments (Hamilton 1976; Bowles 1997; Buckingham 2005), we restrict our consideration of inelasticity to models characterized by uniform attenuation when evaluating the reflection coefficients. This simplification is justified given that preliminary numerical modelling experiments with attenuation profiles based on the pertinent literature (Hamilton 1972, 1976; Spencer 1981; Stoll 1989) have shown that the detailed form of the attenuation–depth curves seem to have only a minor influence on the reflection coefficients. To illustrate the overall impact of an attenuating seabed, we present examples with moderate to pronounced attenuation in the modelling section.

Finally, to separate the velocity effect from the density effect, we keep the density in our models constant at $2100\,\mathrm{kg\,m^{-3}}$. This corresponds to a porosity of ∼35 per cent, which is a reasonable average for the uppermost ∼100 m of a sandy seafloor (e.g. Jackson & Richardson 2007). The resulting seismic macromodels of the sediment-covered seabed considered in this study are summarized in Table 1 and illustrated in graphical form in Fig. 1.

2.2 Fine-scale layering

In clastic marine environments, sand–silt/clay sequences are common and can result from a variety of sedimentation processes (Terwindt *et al.* 1968; Hiemstra *et al.* 2004; Abam 2004; Rotondo 2004). Typically, such sedimentary sequences are scale-invariant, or 'fractal', in nature and exhibit a characteristic hyperbolic or lognormal distribution of the layer thicknesses (Christakos 1992; Turcotte 1997; Holliger & Goff 2003). In the following, we seek to reproduce this property by generating stacks of layers with the above-mentioned stochastic thickness distribution and assign the layers elastic properties that alternate between those of sand and silt/clay at the given depth level. To this end, we generate second-order stationary realizations of a random variable using the von Kármán autocovariance function $C(r)$, which adequately characterizes band-limited scale-invariant phenomena (e.g. von Kármán

Table 1. Velocity–depth functions for end-member models of unconsolidated clastic seabed sediments.

	Sand	Silt/clay
V_P	$V_P(z) = 1800\frac{1}{s} \times z^{0.015}$ (Buckingham 2005; Hamilton 1979)	$V_P(z) = 1511\frac{m}{s} + 1.304\frac{1}{s} \times z$ (Hamilton 1980)
V_S	$V_S(z) = 128\frac{1}{s} \times z^{0.28}$ (Buckingham 2005; Hamilton 1976, 1987)	$V_S(z) = 20.5\frac{1}{s} \times z^{0.4496}$ (Lovell & Odgen 1984; Bowles 1997)

Note: The units used for the depth z and the seismic *P*- and *S*-wave velocities, V_P and V_S, are in m and $\frac{m}{s}$, respectively. See also Fig. 1.

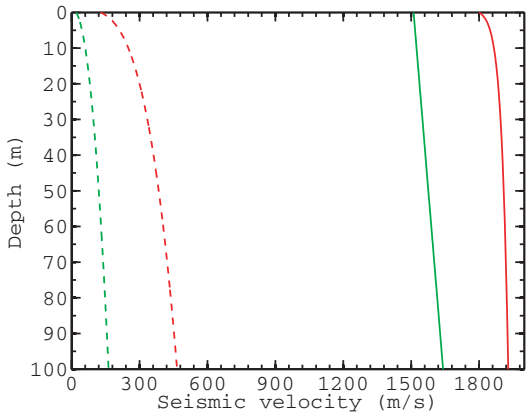

Figure 1. Seismic velocities–depth profiles for sandy (red) and silt/clayey (green) seabeds. Solid lines: *P*-wave velocities; dashed lines: *S*-wave velocities. See also Table 1.

1948; Holliger 1996; Carcione *et al.* 2003)

$$C(r) = \frac{\sigma^2}{2^{\nu-1}\Gamma(\nu)}(r/a)^{\nu}K_{\nu}(r/a). \tag{1}$$

Here, Γ is the gamma function, K_{ν} the modified Bessel function of the second kind of order $0 \leq \nu \leq 1$, r the lag, a the correlation length and σ^2 the variance. The corresponding 1-D power spectrum is given by (e.g. Holliger 1996)

$$P_{hh}(k) = \frac{2\sigma^2\sqrt{a\pi}\,\Gamma\left(\frac{1}{2}+\nu\right)}{\Gamma(\nu)(1+a^2k^2)^{\left(\frac{1}{2}+\nu\right)}}, \tag{2}$$

where k denotes the wavenumber. This indicates that truly scale-invariant or fractal behaviour prevails for $|ka| \gg 1$.

A stochastic process with ν close to zero corresponds to the ubiquitous pink or flicker noise, which seems to universally characterize well logs in general and sonic logs in particular (e.g. Holliger 1996; Ulrych 1999; Hardy & Beier 1994; Kelkar & Perez 2002; Holliger & Goff 2003). To generate a realization of a von-Kármán-type stochastic process, we evaluate the corresponding amplitude spectrum $\sqrt{P_{hh}(k)}$, uniformly randomize its phase, and take the inverse Fourier transform. The resulting data set has a Gaussian probability density function (e.g. Goff & Jordan 1988). For our seafloor models, we generate a stochastic 1-D sequence for a layer thickness characterized by a lognormal distribution with a mean and variance of $\tilde{\mu} = 0.016$ m, $\tilde{\sigma}^2 = 0.0467$ m, respectively, and $\nu = 0.1$ and $a = 100$ m. The lognormal probability density function of our layer sequence is obtained by transforming and rescaling the original Gaussian-distributed data sequence (e.g. Christakos 1992; Lampe & Holliger 2003). We then assign the layers elastic properties, alternating between those of sand and silt/clay at the corresponding depth.

3 EFFECTIVE MODELS OF SAND–SILT/CLAY LAYER SEQUENCES

3.1 Methodology

It is well known that for wavelengths much longer than the prevailing layer thickness, a stack of finely layered isotropic units can be replaced by an effective, transversely isotropic layer (Postma 1955). Vertical transverse isotropy (VTI) is a particular form of seismic anisotropy for which the symmetry axis corresponds to the vertical axis of the model. In this case, the elasticity tensor is characterized by only five independent elastic constants

$$\mathbf{C_{VTI}} = \begin{pmatrix} c_{11} & c_{12} & c_{13} & 0 & 0 & 0 \\ c_{12} & c_{11} & c_{13} & 0 & 0 & 0 \\ c_{13} & c_{13} & c_{33} & 0 & 0 & 0 \\ 0 & 0 & 0 & c_{55} & 0 & 0 \\ 0 & 0 & 0 & 0 & c_{55} & 0 \\ 0 & 0 & 0 & 0 & 0 & c_{66} \end{pmatrix}, \quad 2c_{66} = c_{11} - c_{12}. \tag{3}$$

VTI adequately represents the seismic characteristics of a horizontally layered medium, is computationally relatively easy to handle, and is therefore popular for modelling purposes (Le Stunff *et al.* 2001; Lynn 2004). Comprehensive reviews of seismic anisotropy in general and VTI in particular are provided, for example, by Tsvankin (2005) and Carcione (2007).

As it is difficult to get an intuitive understanding of the anisotropy of a medium based on its elasticity tensor, it is common practice to use the notation introduced by Thomsen (1986) to describe VTI media. The basic idea behind this is to separate the anisotropic influence on the isotropic *P*- and *S*-wave quantities using three dimensionless parameters

$$\epsilon = \frac{c_{11} - c_{33}}{2c_{33}}, \tag{4}$$

$$\delta^{\star} = \frac{1}{2c_{33}^2}\left[2(c_{13}+c_{55})^2 - (c_{33}-c_{55})(c_{11}+c_{33}-2c_{55})\right], \tag{5}$$

$$\gamma = \frac{c_{66} - c_{55}}{2c_{55}}. \tag{6}$$

The parameters ϵ and γ provide indications of the differences between horizontal and vertical *P*- and *SH*-wave velocities, respectively. $\delta^{\star}$ corresponds to the second derivative of the *P*-wave velocity at normal incidence and thus describes the anisotropic behaviour at near-vertical incidence angles (Tsvankin & Thomsen 1994). All parameters are zero for isotropic materials. Sidler & Carcione (2007) investigated the behaviour of the *P*-wave reflection coefficient due to anisotropy controlled by the Thomsen parameters. They found that in terms of *P*-wave reflection, the coefficient ϵ controls steeply incident waves and increases or decreases the reflection coefficient in the pre-critical range, whereas δ most influences the critical and post-critical range where the change of amplitude is most pronounced, especially in combination with attenuation.

The seismic seabed models derived above have velocity gradients that are especially prominent at shallow depths, which in turn result in a corresponding depth-dependence of the dominant seismic wavelength. This is important because the long-wavelength-equivalent approximation is valid only for wavelengths substantially longer than the evaluated layer sequence. The ratio between the dominant wavelength λ and the effective layer thickness d

$$R = \frac{\lambda}{d} \tag{7}$$

was estimated to be in the range between five to eight for a periodic layer sequence (Postma 1955; Carcione *et al.* 1991), and more than eight for stochastic layer sequences (Carcione 2007). This is illustrated in Fig. 2, which shows velocity–depth profiles for different values of R based on 10 stochastic realizations of the *P*-wave velocity. We see that there is no clear threshold and that a value of R around 10 is a good approximation. Much smaller or much larger values of R can be clearly identified as either oversimplifying the

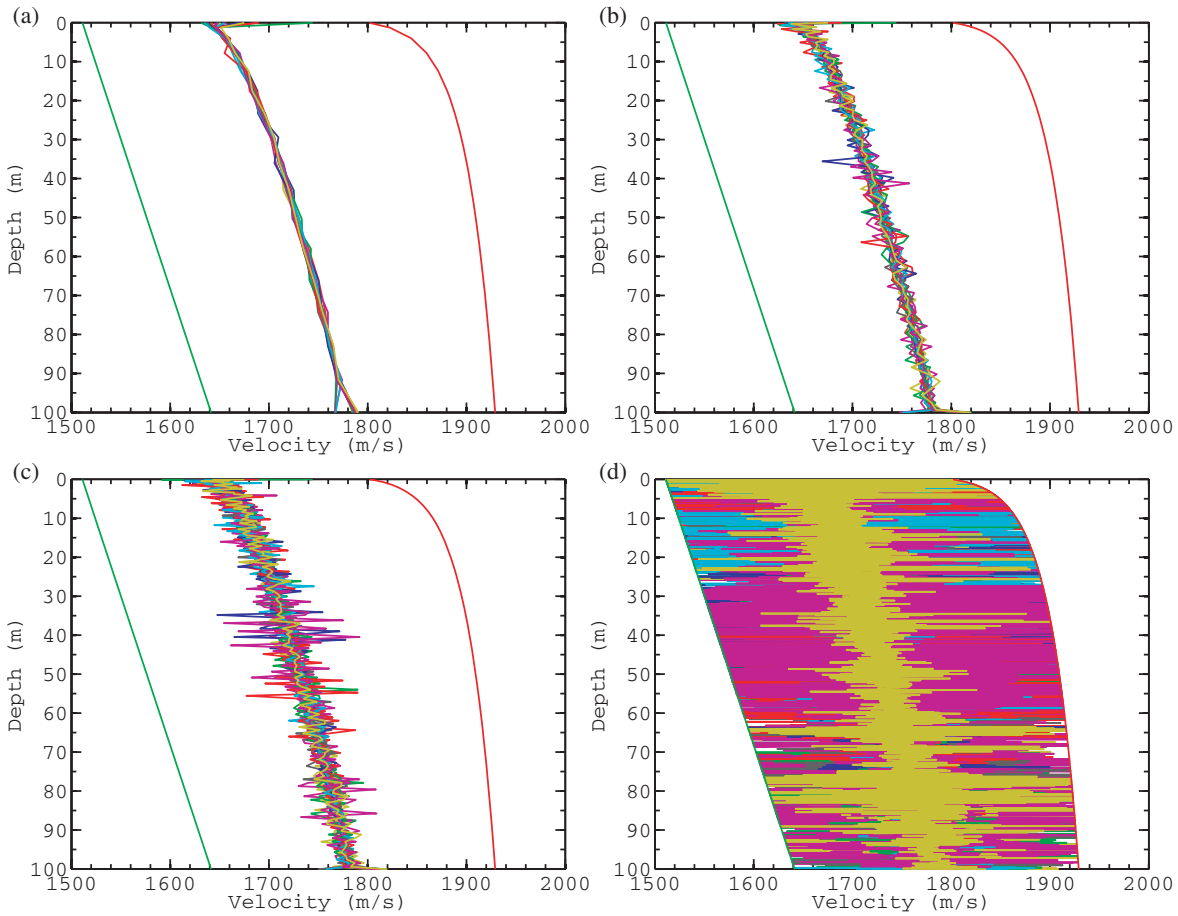

Figure 2. Ten realizations of the *P*-wave velocity for the same stochastic layer sequence with different effective media averaging values *R*. (a) $R = 1$, (b) $R = 5$, (c) $R = 10$ and (d) $R = 100$. The red and green lines corresponds to the sand and silt/clay end-member models, respectively.

underlying heterogeneity or as being inefficient. Moreover, Fig. 2 illustrates that a too coarse sampling of finely layered sediments leads to an underestimation of the heterogeneity and, consequently, also to an underestimation of the variability of the anisotropy (e.g. Sams 1995).

To estimate the seismic characteristics of the stochastic layer sequence described earlier, we set up a substitute layer stack in which the layers have a thickness of one tenth of the dominant wavelength. We consider a dominant frequency of 35 Hz, which is typical for marine seismic exploration data, and use the higher velocity of our bimodal distribution. Using effective media theory, we then replace the isotropic sand and silt/clay layers from our geological model with anisotropic layers with an equivalent seismic response

$$\begin{aligned} c_{11} &= \left\langle c_{11} - c_{13}^2 c_{33}^{-1} \right\rangle + \left\langle c_{33}^{-1} \right\rangle^{-1} \left\langle c_{33}^{-1} c_{13} \right\rangle^2, \\ c_{33} &= \left\langle c_{33}^{-1} \right\rangle^{-1}, \\ c_{13} &= \left\langle c_{33}^{-1} \right\rangle^{-1} \left\langle c_{33}^{-1} c_{13} \right\rangle, \\ c_{55} &= \left\langle c_{55}^{-1} \right\rangle^{-1}, \\ c_{66} &= \langle c_{66} \rangle, \end{aligned} \tag{8}$$

where the weighted average of L different components is defined as

$$\langle a \rangle = \sum_{l=1}^{L} p_l a_l \tag{9}$$

with p_l denoting the fractional proportion of component a_l. The global process of creating a stochastic layer sequence, assigning material properties to the layers, and estimating the material properties of equivalent layers with a tenth of the wavelength at a given depth using effective media theory (Backus 1962; Schoenberg & Muir 1989) is schematically illustrated in Fig. 3.

An inherent property of a stochastic variable is that an infinite number of realizations are possible. In the following, we therefore calculate the elastic equivalent of 100 different realizations of stochastic layer sequences and extract the mean values and standard deviations for the *P*- and *S*-wave velocities as well as for the three Thomsen parameters ϵ, δ and γ. For vertically travelling waves, the *P*- and *SV*-wave velocities of the transversely isotropic medium are given as

$$V_P = \sqrt{c_{33}/\rho}, \tag{10}$$

$$V_{SV} = \sqrt{c_{55}/\rho}, \tag{11}$$

where ρ denotes the density. In directions other than vertical, the velocities vary depending on the prevailing anisotropy. The mean of all realizations corresponds to an alternating layer sequence with uniform layer thickness according to the average layer thickness of the stochastic layer sequence.

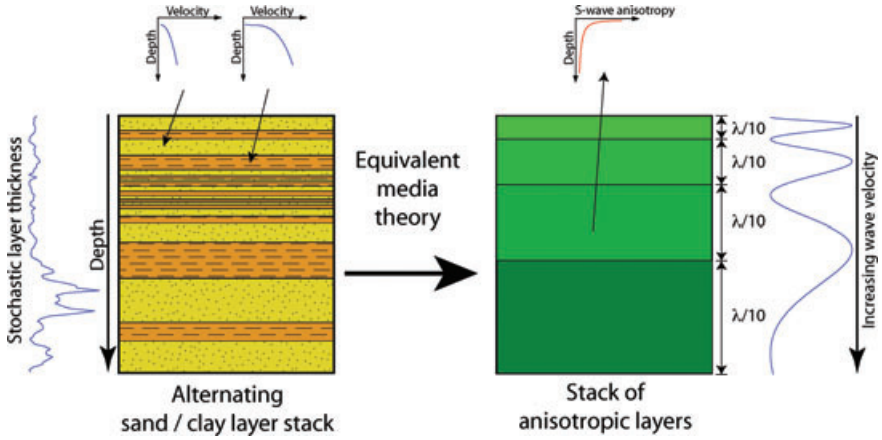

Figure 3. Schematic illustration of the assignment of a stochastic layer sequence and seismic material properties to the layers (left) as well as the estimation of anisotropy using effective media theory (right). Because of the constraint of effective media theory being valid only for layers substantially smaller than the dominant wavelength λ, the thickness of the resulting set of anisotropic layers is chosen to be a tenth of the wavelength of the faster component. The length of this averaging interval increases systematically with depth in response to the correspondingly increasing seismic velocity and wavelength.

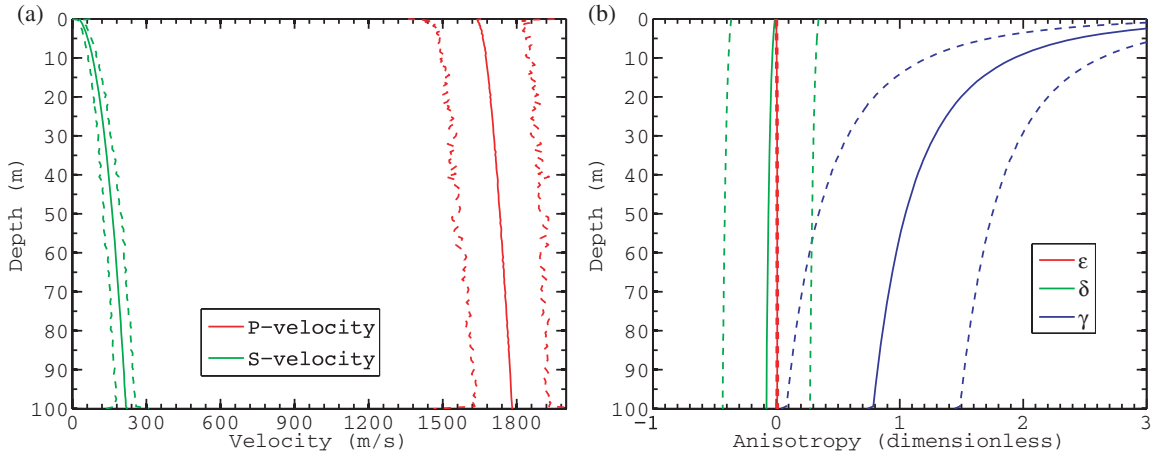

Figure 4. Mean values (solid lines) and standard deviations (dashed lines) of the (a) *P*-wave and *S*-wave velocities and (b) the corresponding Thomsen parameters ϵ, δ, and γ for the effective transversely isotropic model with $R = 10$ based on 100 different realizations of stochastic sand–silt/clay layer sequences. Here, the silt/clay layers are isotropic.

3.2 Application to sand–silt/clay layer sequences

To isolate the effects of thin layering on the seismic anisotropy of the surficial seabed from those related to intrinsic anisotropy, we assume that the silt/clay layers are isotropic for our first suite of stochastic models. Practically, this assumption corresponds to the relatively common case of an interlayering of sand and silt or non-mineralogical, granulometric clay. The mean and standard deviation of the seismic velocities of the equivalent medium are shown in Fig. 4(a). Fig. 4(b) shows the Thomsen parameters for the effective medium together with their standard deviations. The parameter ϵ is zero for the entire depth range considered, δ is small and largely invariant, whereas γ is characterized by large variations with high values at the ocean bottom and a rapid decrease along with depth. γ is significantly larger than the other anisotropy parameters and its variation for different realizations of the stochastic velocity models is quite significant.

Based on these parameters and the fact that γ is controlling the elliptical anisotropy of the *SH*-wavefield, which, for the VTI case is entirely decoupled from the *qP*-*SV*-wavefield, it is not immediately obvious whether our seafloor model supports *SV*-wave triplications. Thomsen & Dellinger (2003) address this question by comparing an approximative parameter σ_{critical} with the corresponding anisotropy parameter σ (Tsvankin & Thomsen 1994) and conclude that if the condition

$$\frac{c_{33}}{c_{55}}(\epsilon - \delta) \equiv \sigma > \sigma_{\text{critical}} \equiv \frac{2}{3}\left(1 + \delta - \frac{c_{55}}{9c_{33}}\right) \tag{12}$$

is fulfilled, *SV*-triplication do indeed exist. This implies that, for a certain range of propagation angles, the medium supports three different group velocities (Dellinger 1991; Zhou & Greenhalgh 2004). Eq. (12) indicates that the occurrence of *SV*-waves triplications is strongly related to the vertical *P*-to-*S*-wave velocity ratio given by $\sqrt{c_{33}/c_{55}}$ (see eqs 10 and 11), which is inherently very high for soft surficial seabed sediments (Table 1; Fig. 1). Figs 5(a) and (b) show the group velocities of the *P*- and *S*-waves and the corresponding polarization at the ocean bottom for the considered seabed model. Evaluation of the condition for triplications (eq. 12) indicates a large disequilibrium which indeed results in triplications for all propagation angles that are more than 8° off the axis (Fig. 5b). Please note that the angular range for *SV*-triplications lies between the cusps of the group velocity curve and that the corresponding minimum

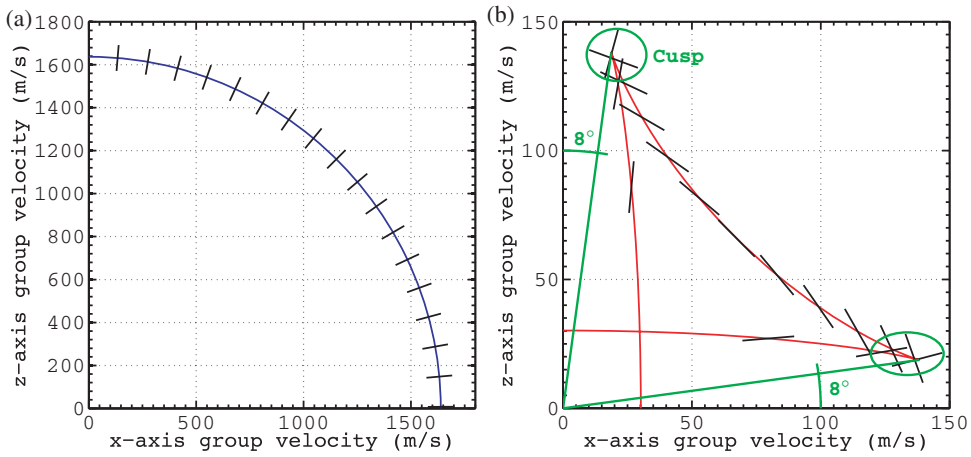

Figure 5. Group velocities at the seabed for (a) *P*- (blue) and (b) *S*-waves (red) for the VTI effective medium corresponding to a regularly layered sand–silt/clay sequence characterized by the velocity gradients given in Table 1. The silt/clay layers are assumed to be devoid of any intrinsic anisotropy. The polarization is denoted by black line segments and is displayed at angular intervals of five degrees.

angle is defined as the angle between the z-axis and the line connecting the origin with the cusp. Conversely, our effective medium does not fulfill the condition for anomalous polarization (Helbig & Schoenberg 1987)

$$c_{13} + c_{44} < 0. \tag{13}$$

While the intrinsic anisotropy of sand, silt and non-mineralogical clay is considered to be quite benign due to the random orientation of the predominantly round grains (e.g. Carlson *et al.* 1984), the intrinsic anisotropy of mineralogical clay is generally very important (e.g. Wang 2002). In our second stochastic layer sequence, we account for this phenomenon and use the Thomsen parameters derived by Bayuk *et al.* (2007) ($\epsilon = 0.89$, $\gamma = 3.1$ and $\delta = -0.34$) to model the effect of the intrinsic anisotropy of the clay layers. The corresponding results are shown in Figs 6(a) and (b) for the seismic velocities and Thomsen parameters, respectively. The anisotropy of individual realizations quantified by δ and γ becomes less erratic resulting in a smaller standard deviation, although the mean values are about twice as large as for the purely isotropic layering (Figs 4 and 6). ϵ shows higher values over the entire depth range. The *P*- and *SV*-wave group velocities of this medium as well as the corresponding polarizations are shown in Fig. 7. Because of the large anisotropy, the *SV*-wave velocities off the x–z axes are substantially larger than along the axes and *SV*-wave triplications occur already for *S*-waves propagating at angles differing more than 1° from vertical. As in the previously considered case of uniformely isotropic layering, the condition for anomalous polarization (eq. 13) is, however, not fulfilled.

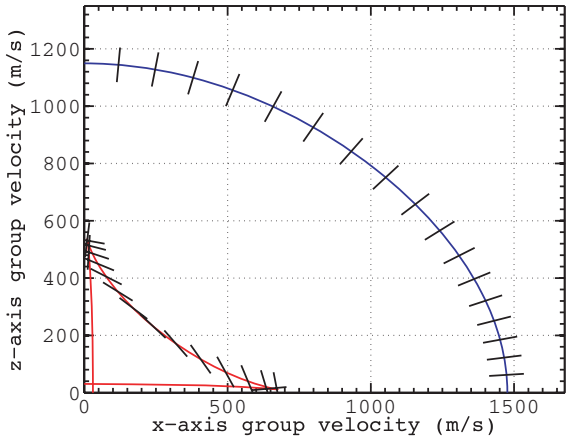

Figure 7. Same as Fig. 5, except that the clay layers are assumed to be intrinsically anisotropic ($\epsilon = 0.89$, $\gamma = 3.10$, $\delta = -0.34$).

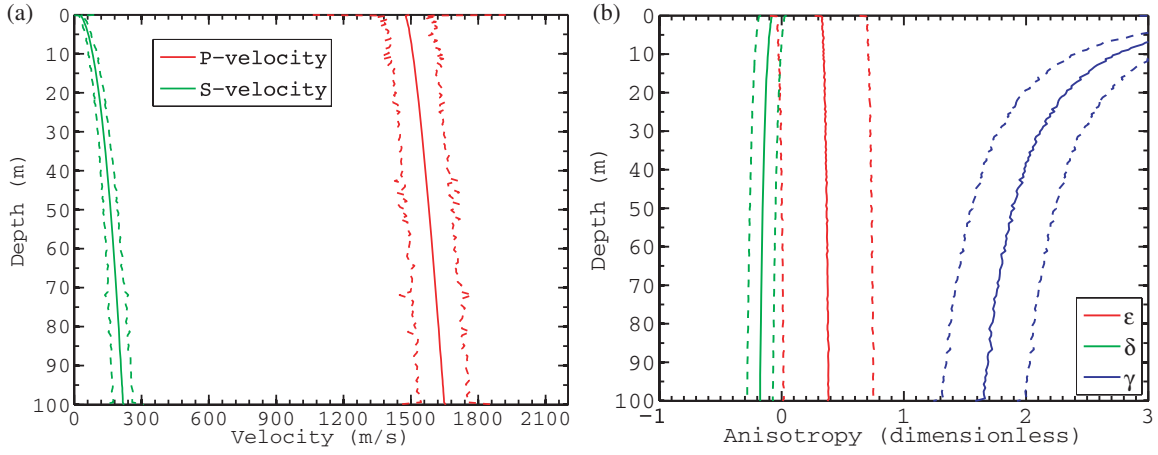

Figure 6. Same as Fig. 4, except that the clay layers are assumed to be intrinsically anisotropic ($\epsilon = 0.89$, $\gamma = 3.10$, $\delta = -0.34$).

4 MODELLING OF SEABED REFLECTION COEFFICIENTS

For the seismic models considered in this study, we focus on downgoing waves reflected from the seabed back into the water column and the reflection coefficient is therefore defined as the ratio between the incident and reflected pressure as a function of the incidence angle. In contrast to most other seismic attributes, measuring the reflection coefficient is, at least in principle, relatively straightforward. Conversely, the analytical evaluation of reflection coefficients based on the plane-wave approximation tends to be rather cumbersome in general and particularly so for inelastic and for anisotropic media (Aki & Richards 1980; Krebes & Daley 2007; Sidler *et al.* 2008). Moreover, analytical approaches for the evaluation of reflection coefficients are limited to relatively simple, and hence often unrealistic, models. Carcione & Helle (2004) and Sidler & Carcione (2007) did, however, show that reflection coefficients calculated with the plane-wave approximation agree well with reflection coefficients extracted from corresponding numerical wavefield simulations with a special treatment of interfaces (Carcione 1991; Tessmer *et al.* 1992; Carcione 1996). In the following, we evaluate the numerical reflection coefficients calculated for four models representative of the range of seismic seabed models considered in this study and compare the results with the corresponding plane-wave reflection coefficients for equivalent homogeneous half-space models. The latter are defined by the seismic properties at the top of the corresponding heterogeneous models. We use the frequency-slowness method to evaluate the reflection coefficients from seismograms that are numerically obtained with a pseudo-spectral modelling code (Kreiss & Oliger 1972; Orszag 1972; Fornberg 1975, 1987; Tessmer *et al.* 1992; Carcione 2007). In principle, the numerical reflection coefficient is evaluated at the centre frequency of the considered source spectrum. To allow for a denser sampling of the pertinent range of incidence angles, we did, however, consider the composite solution for three individual frequencies in the immediate vicinity of the centre frequency. A detailed description of the frequency-slowness method for estimating the numerical reflection coefficients as well as the equations for evaluating the analytical plane-wave reflection coefficients can be found in Sidler *et al.* (2008).

In the first example, we investigate the influence of the typically very pronounced vertical velocity gradients in the surficial seabed on the reflection coefficient. Fig. 8(a) shows the amplitude, or absolute value, of the generally complex-valued reflection coefficient for a homogeneous half-space with the elastic properties of sand on top of the seabed. For this model, we can directly compute the corresponding analytical plane-wave reflection coefficient, which agrees well with the numerical solution and thus illustrates the adequacy of this approach. For comparison, we also show the analytical plane-wave reflection coefficient for a corresponding moderately

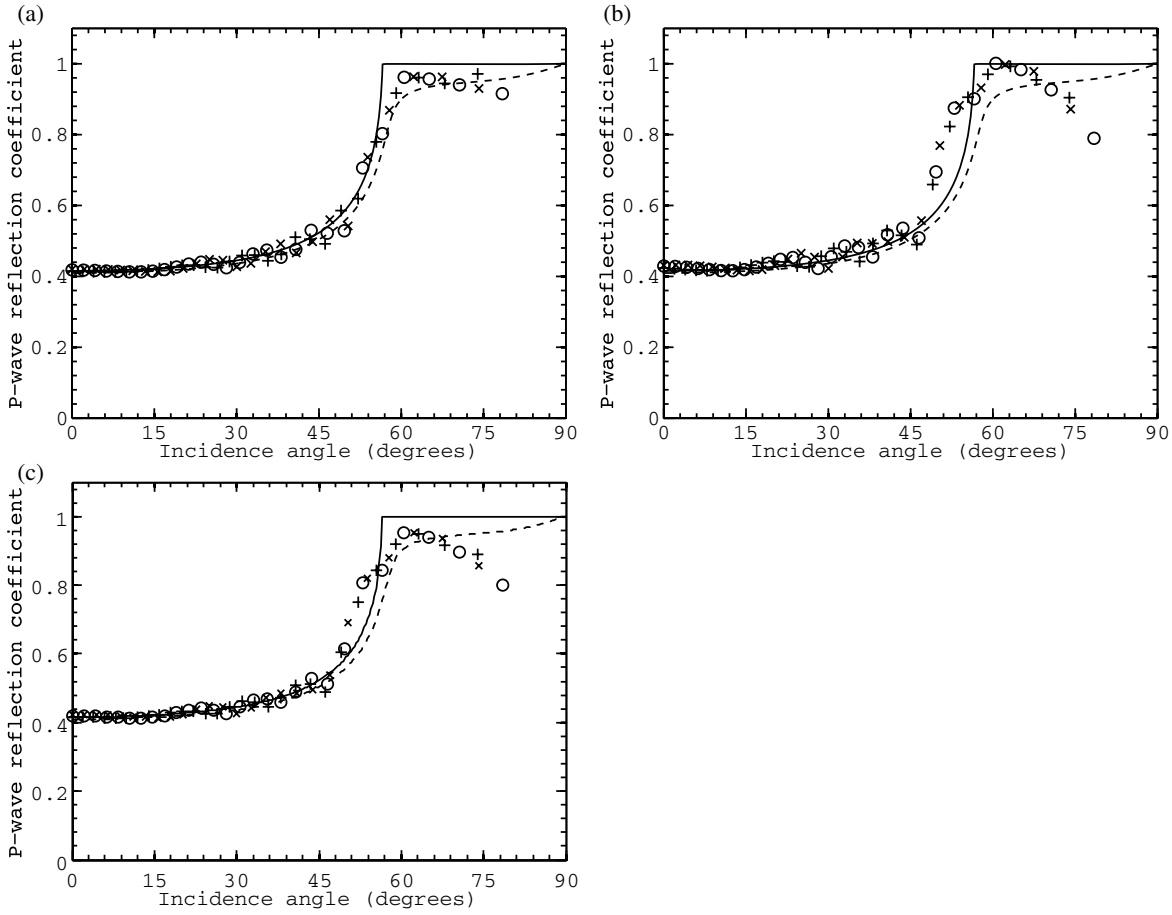

Figure 8. Absolute values of reflection coefficients for a sandy seabed model. (a) Numerical reflection coefficient for a homogeneous half-space with constant velocities ($V_P = 1800\,\mathrm{m\,s^{-1}}$, $V_S = 128\,\mathrm{m\,s^{-1}}$); (b) numerical reflection coefficient for an elastic model with the vertical velocity gradient of a sandy seabed from Table 1; (c) same as (b) but characterized by moderate attenuation ($Q_P = 34$; $Q_S = 25$). Symbols represent the numerical solutions at 34, 36 and 37 Hz. The solid and dashed lines correspond to the analytical elastic and viscoelastic plane-wave reflection coefficients, respectively.

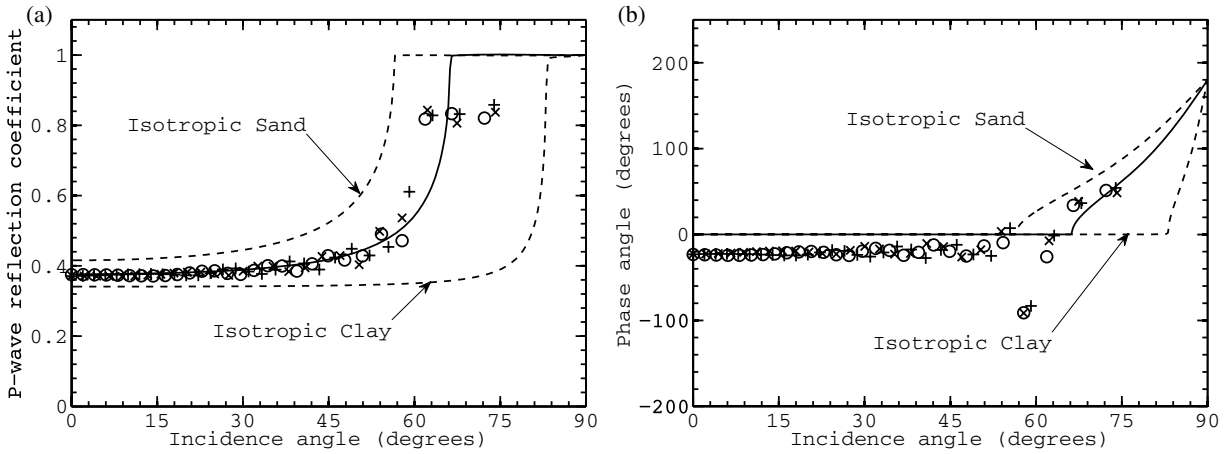

Figure 9. (a) Amplitude and (b) phase of the numerical reflection coefficient for the elastic effective seabed model of a finely layered sand–silt/clay sequence with stochastically distributed layer thicknesses. The properties of this medium correspond to the values in Fig. 4. Symbols correspond to the numerical solutions at 34, 36 and 37 Hz. The dashed lines correspond to models comprising elastic sand and silt/clay half-spaces. The solid line corresponds to the best-fitting solution, in a non-weighted least-squares sense, when inverting the numerical result using an analytical elastic plane-wave solution yielding the following parameters: $V_P = 1640\,\mathrm{m\,s^{-1}}$, $V_S = 90\,\mathrm{m\,s^{-1}}$ and $\rho = 2100\,\mathrm{kg\,m^{-3}}$.

attenuating, viscoelastic seabed characterized by *P*- and *S*-wave quality factors of $Q_P = 34$ and $Q_S = 25$, respectively. The resulting differences with regard to the elastic case are negligible in the pre-critical range and minor in the critical and post-critical ranges. Next, we introduce a vertical velocity gradient in the seabed of the kind given in Table 1 and illustrated in Fig. 1 for the numerical solution and compare it to the plane-wave solution for the corresponding homogeneous half-space model (Fig. 8b). Here, it is important to note that the elastic parameters at the seabed are the same as for the homogeneous model (Fig. 8a). The numerical solution shows a clear difference with regard to the analytical solution for the homogeneous half-space model in the vicinity of the critical angle and in the post-critical range (Fig. 8b). Although numerical artifacts cannot be entirely excluded at such large incidence angles, the decreasing reflection coefficient beyond the critical angle is likely to be a physical reality indicating stronger transmission of the incident seismic energy into the seabed in response to the vertical velocity gradient. Conversely, the additional effects caused by attenuation shown in Fig. 8(c) are relatively benign, as would indeed be expected based on the results obtained for the corresponding half-space model (Fig. 8a).

Fig. 9 shows the amplitude and phase of the numerical reflection coefficient of the effective model for stochastic sand-silt/clay layer sequences. We again first ignore the potential intrinsic anisotropy of the clay layers and the elastic properties of this model thus correspond to that shown in Fig. 4. The thus resulting reflection coefficient lies between the values for the corresponding homogenous sand and silt/clay half-space models. Linearized least-squares inversion of the numerical reflection coefficient for the best-fitting elastic half-space model yields $V_P = 1640\,\mathrm{m\,s^{-1}}$ and $V_S = 90\,\mathrm{m\,s^{-1}}$. The estimated *P*-wave velocity agrees well with the true *P*-wave velocity of $1650\,\mathrm{m\,s^{-1}}$ at the water–sediment interface, whereas the inferred *S*-wave velocity is overestimated by some 100 per cent. The phase of the reflection coefficient shows a discontinuity at the critical angle. This phase jump, which is not present in the homogeneous analytical model, was found to be absent in the isotropic gradient model for the sandy seafloor discussed earlier and could therefore be related to the transversely isotropic velocity gradient.

To explore the seismic effects of a strongly attenuating seafloor, we also evaluated the reflection coefficient for a corresponding model characterized by $Q_P = Q_S = 15$. Based on the available evidence, such a strong attenuation does, however, seem to be relatively uncommon in surficial seabed sediments (Hamilton 1972; Bowles 1997). The results shown in Fig. 10 indicate that the amplitude of the reflection coefficient is only slightly lower than for the corresponding elastic model (Fig. 9) in the pre-critical range. At larger incidence angles, the reflected amplitude is, however, dramatically lower compared to the corresponding elastic model (Figs 9a and 10a). An additional interesting observation is that the phase jump present in the elastic model (Fig. 9b) vanishes in the presence of strong attenuation (Fig. 10b).

In our final model, we account for the intrinsic anisotropy of the clay layers in the stochastic layer sequence, and the elastic properties of the ocean bottom thus correspond to those shown in Fig. 6. The resulting amplitude and phase of the reflection coefficient are shown in Fig. 11, which illustrates that, for this configuration of seismic material parameters, the seabed is highly transmissive and only a small fraction of the incident energy is reflected. Moreover, the reflection coefficient exhibits only a weak variation with incidence angle and its overall character and shape are completely different from those of the pertinent elastic half-space models. Therefore, not surprisingly, the unconstrained and non-weighted inversion of the reflection coefficient for the best-fitting elastic half-space model, which yields $V_P = 1430\,\mathrm{m\,s^{-1}}$, $V_S = 210\,\mathrm{m\,s^{-1}}$, neither provides a good fit to the observed data nor an adequate approximation of the actual seismic properties at the top of the sedimentary pile ($V_P \cong 1650\,\mathrm{m\,s^{-1}}$, $V_S \cong 30\,\mathrm{m\,s^{-1}}$). Here again, it is important to note that the error in the estimation of the *P*-wave velocity in the immediate vicinity of the seabed is quite moderate ($\sim$15 per cent), whereas the corresponding *S*-wave velocity estimate is off by almost one order-of-magnitude.

Sedimentary layering in the surficial seabed thus seems to influence *S*-wave propagation considerably more strongly than *P*-wave propagation. Changes in the *P*-wave reflection coefficients due to fine layering and velocity gradients with regard to the corresponding isotropic homogeneous half-space model are rather moderate and primarily restricted to larger incidence angles, where *P*-wave

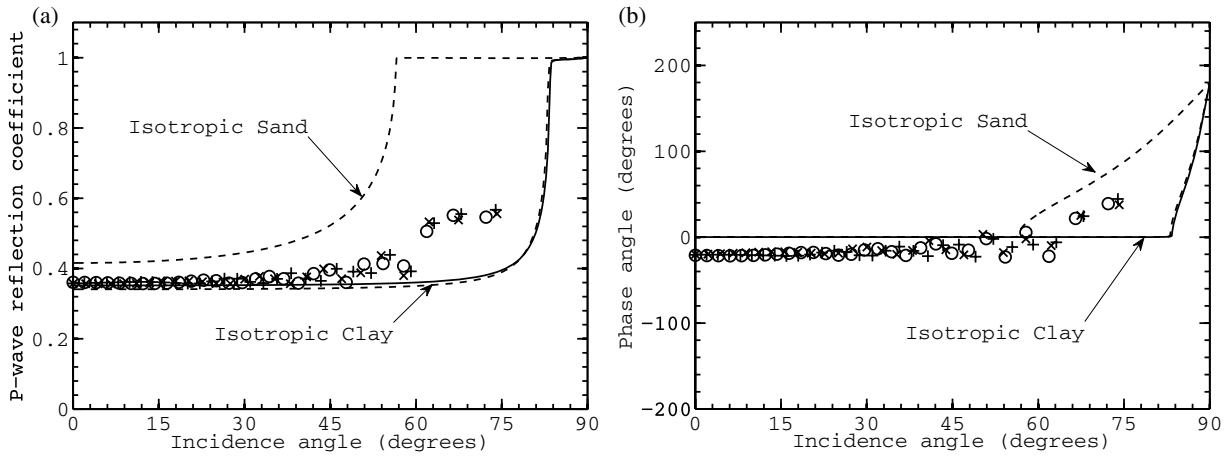

Figure 10. (a) Amplitude and (b) phase of the numerical reflection coefficient for the effective seabed model for a finely layered sand–silt/clay sequence characterized by stochastically distributed layer thicknesses with strong attenuation ($Q_P = Q_S = 15$). Symbols correspond to the numerical solutions at 34, 36 and 37 Hz. The dashed lines correspond to analytic reflection coefficients for seabed models consisting of sand and silt/clay half-spaces. The solid line denotes to the best-fitting analytical solution, in a non-weighted least-squares sense, corresponding to an elastic and isotropic model characterized by $V_P = 1510\,\mathrm{m\,s^{-1}}$, $V_S = 29\,\mathrm{m\,s^{-1}}$ and $\rho = 2155\,\mathrm{kg\,m^{-3}}$.

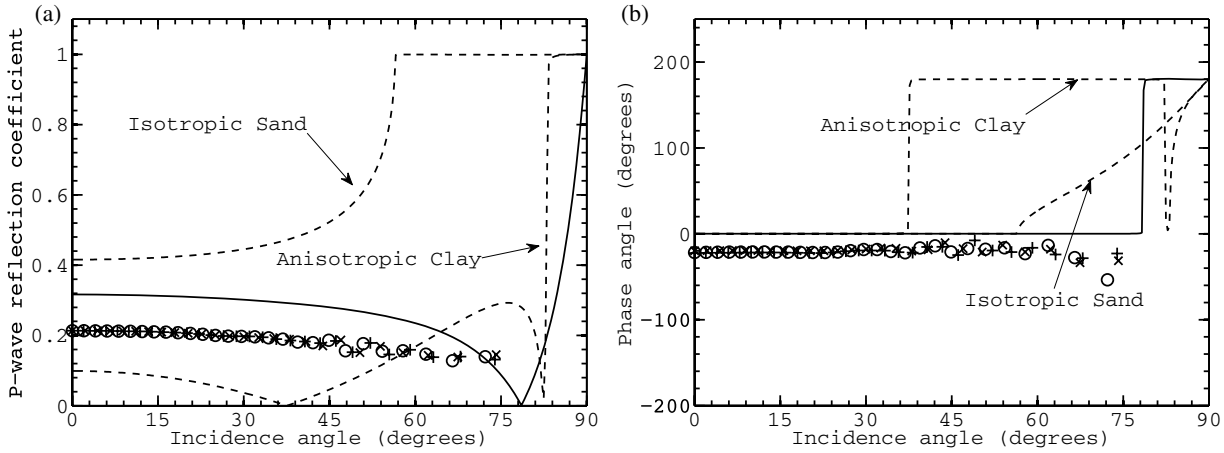

Figure 11. (a) Amplitude and (b) phase of the numerical reflection coefficient for the effective seabed model of a finely layered sand–clay sequence with stochastically distributed layer thicknesses and intrinsic anisotropy of the clay layers. The properties of this medium correspond to those in Fig. 6. Symbols represent the numerical solutions at 34, 36 and 37 Hz, respectively. The dashed lines correspond to seabed models characterized by homogeneous and elastic sand and clay half-spaces. The solid line is the best-fitting solution, in a non-weighted least-squares sense, when inverting the numerical results using analytical elastic plane-wave solution yielding the following parameters: $V_P = 1430\,\mathrm{m\,s^{-1}}$, $V_S = 210\,\mathrm{m\,s^{-1}}$ and $\rho = 2100\,\mathrm{kg\,m^{-3}}$.

transmission is reduced and *S*-wave conversion becomes the controlling mechanism. Our results thus indicate that for certain, arguably reasonably realistic, models of the sediment-covered seabed the inverse problem for the estimation of the seismic properties based on the elastic *P*-wave reflection coefficient is inherently ill-posed.

5 CONCLUSIONS

We have constructed realistic seismic models of a surficial seabed covered by unconsolidated clastic sediments and explored the implications arising for seismic wave propagation in general and seafloor reflectivity in particular. In doing so, we made a concerted effort to constrain the amount of seismic anisotropy that could potentially be present in the surficial seabed due to the interlayering of sand and silt/clay, which are the most common types of clastic marine sediments. The corresponding results indicate that anisotropy is rather benign for *P*-waves but does have a pronounced impact on the propagation of *S*-waves. We found the layered media considered in this study to exhibit *S*-wave triplications at propagation angles as low as 8° and 1° off the axes for uniformly isotropic layers and intrinsically anisotropic clay layers, respectively. We also found that a seafloor containing intrinsically anisotropic clay layers tends to transmit most of incident seismic energy. In such cases, the reflection coefficient varies only weakly with incidence angle and a critical angle cannot be clearly identified. The large *S*-wave anisotropy in combination with the moderate *P*-wave anisotropy resulting from our models indicate that the estimation of *S*-wave velocity in the immediate vicinity of the seabed based on analytical models of the *P*-wave reflection coefficient is in many, if not most, cases likely to be inadequate. Conversely, our results also indicate that corresponding estimates of the *P*-wave velocity are in general remarkably accurate and robust.

ACKNOWLEDGMENTS

The authors are grateful to Stewart Greenhalgh, the editor Michael Diament and two anonymous referees whose comments and

suggestions helped to improve the quality of this paper. We also thank José Carcione for discussions and for providing his pseudo-spectral modelling code, the Applied and Environmental Geophysics Group at the ETH Zurich for allowing us to use their computing facilities, and Carey Sargent for editing the text of this manuscript. This work has been supported by EU grant MRTN-CT-2003-504267 as well as by a grant from the Swiss National Science Foundation.

REFERENCES

Abam, T.K.S., 2004. Case histories of sand search in the niger delta, *Environ. Geol.,* **46,** 165–172.

Aki, K. & Richards, P.G., 1980. *Quantitative Seismology,* W.H. Freeman, New York.

Amundsen, L. & Reitan, A., 1995. Decomposition of multicomponent seafloor data into upgoing and downgoing P- and S-waves, *Geophysics,* **60,** 563–572.

Bachman, R.T., 1979. Acoustic anisotropy in marine sediments and sedimentary rocks, *J. geophys. Res.,* **84,** 7661–7663.

Bachman, R.T., 1983. Elastic anisotropy in marine sedimentary rocks, *J. geophys. Res.,* **88,** 539–545.

Backus, G.E., 1962. Long-wave elastic anisotropy produced by horizontal layering, *J. geophys. Res.,* **67,** 4427.

Banik, N.C., 1984. Velocity anisotropy of shales and depth estimation in the North Sea basin, *Geophysics,* **49,** 1411–1419.

Bayuk, I.O., Ammerman, M. & Chesnokov, E.M., 2007. Elastic moduli of anisotropic clay, *Geophysics,* **72,** D107–D117.

Berge, P.A., Mallick, S., Fryer, G.J., Barstow, N., Carter, J.A., Sutton, G.H. & Ewing, J.I., 1991. In situ measurement of transverse isotropy in shallow-water marine sediments, *Geophys. J. Int.,* **104,** 241–254.

Bowles, F.A., 1997. Observations on attenuation and shear-wave velocity in fine-grained, marine sediments, *J. Acoust. soc. Am.,* **101,** 3385–3397.

Bryan, G.M. & Stoll, R.D., 1988. The dynamic shear modulus of marine sediments, *J. Acoust. soc. Am.,* **83,** 2159–2164.

Buckingham, M.J., 2005. Compressional and shear wave properties of marine sediments: Comparisons between theory and data, *J. Acoust. soc. Am.,* **117,** 137–152.

Caldwell, J., 1999. Marine multicomponent seismology, *Leading Edge,* **18,** 1274–1282.

Carcione, J.M., 1991. Domain decomposition for wave propagation problems, *J. Sci. Comput.,* **6,** 453–472.

Carcione, J.M., 1996. A 2D Chebyshev differential operator for the elastic wave equation, *Comput. Methods Appl. Mech. Eng.,* **130,** 33–45.

Carcione, J.M., 2007. *Wave fields in Real Media: Wave Propagation in Anisotropic, Anelastic, Porous and Electromagnetic Media*. 2nd edn, Elsevier, Amsterdam.

Carcione, J.M. & Helle, H.B., 2004. On the physics and simulation of wave propagation at the ocean bottom, *Geophysics,* **69,** 825–839.

Carcione, J.M., Kosloff, D. & Behle, A., 1991. Long-wave anisotropy in stratified media: A numerical test, *Geophysics,* **56,** 245–254.

Carcione, J.M., Finetti, I. & Gei, D., 2003. Seismic modeling study of the earth's deep crust, *Geophysics,* **68,** 656–664.

Carlson, R.L., Schaftenaar, C.H. & Moore, R.P., 1984. Causes of compressional-wave anisotropy in carbonate-bearing, deep-sea sediments, *Geophysics,* **49,** 525–532.

Christakos, G., 1992. *Random Field Models in Earth Sciences,* Academic Press, San Diego.

Dellinger, J., 1991. Anisotropic seismic wave propagation, *PhD thesis*, Stanford University.

Edme, P. & Singh, S.C., 2008. Receiver function method in reflection seismology, *Geophys. Prospect.,* **56,** 327–340.

Edme, P. & Singh, S.C., 2009. Receiver function decomposition of OBC data: Theory, *Geophys. J. Int.,* **177,** 966–977.

Edme, P., Soudani, M., Boelle, J. & Singh, S.C., 2005. Data-driven P-S separation in OBC data, in *OBC data: EAGE/SEG Reasearch Workshop, Pau, France*.

Eggenberger, K., Muijs, R., Robertsson, J.O.A., van Maanen, D.-J. & Holliger, K., 2005. Effects of an anelastic seafloor on the decomposition of marine multi-component seismic data, in *EAGE/SEG Research Workshop, Pau, France*.

Fornberg, B., 1975. On a Fourier method for the integration of hyperbolic equations, *SIAM J. Numer. Anal.,* **12,** 509–528.

Fornberg, B., 1987. The pseudospectral method: comparison with finite differences for the elastic wave equation, *Geophysics,* **52,** 483–501.

Goff, J.A. & Jordan, T.H., 1988. Stochastic modeling of seafloor morphology: Inversion of sea beam data for second-order statistics, *J. geophys. Res.,* **93,** 13 589–13 608.

Hamilton, E.L., 1972. Compressional-wave attenuation in marine sediments, *Geophysics,* **37,** 620–546.

Hamilton, E.L., 1976. Shear-wave velocity versus depth in marine sediments: a review, *Geophysics,* **41,** 985–996.

Hamilton, E.L., 1979. Sound velocity gradients in marine sediments, *J. Acoust. soc. Am.,* **65,** 909–922.

Hamilton, E.L., 1980. Geoacoustical modeling of the sea floor, *J. Acoust. soc. Am.,* **68,** 1313–1340.

Hamilton, E.L., 1987. Acoustic properties of sediments, in *Acoustics and Ocean Bottom,* pp. 3–58, Sociedad Espanol de Acoustica, Madrid, Spain.

Hardy, H. & Beier, R.A., 1994. *Fractals in Reservoir Engineering,* World Scientific, Singapore.

Helbig, K. & Schoenberg, M., 1987. Anomalous polarization of elastic waves in transverse isotropic media, *J. Acoust. soc. Am.,* **81,** 1235–1245.

Hiemstra, J.F., Zaniewski, K., Powell, R.D. & Cowan, E.A., 2004. Strain signatures of fjord sediment sliding: micro-scale examples from Yakutat Bay and Glacier Bay, Alaska. U.S.A., *J. Sedim. Res.,* **74,** 760–769.

Holliger, K., 1996. Upper crustal seismic velocity heterogeneity as derived from a variety of P-wave sonic logs, *Geophys. J. Int.,* **125,** 813–829.

Holliger, K. & Goff, J.A., 2003. A generic model for the 1/f-scaling nature of seismic velocity fluctuations, in *Heterogenity in the Crust and Upper Mantle – Nature, Scaling and Seismic Properties,* pp. 131–154, Kluwer Academic/Plenum Publishers, New York.

Hornby, B.E., Schwartz, L.M. & Hudson, J.A., 1994. Anisotropic effective-medium modeling of the elastic properties of shales, *Geophysics,* **59,** 1570–1583.

Jackson, D.R. & Richardson, M.D., 2007. *High-Frequency Seafloor Acoustics,* Springer, New York.

Kelkar, M. & Perez, G., 2002. *Applied Geostatistics for Reservoir Characterization,* Society of Petroleum Engineers, Richardson, Texas.

Krebes, E.S. & Daley, P.F., 2007. Difficulties with computing anelastic plane-wave reflection and transmission coefficients, *Geophys. J. Int.,* **170,** 205–216.

Kreiss, H.O. & Oliger, J., 1972. Comparison of accurate methods for the integration of hyperbolic equations, *Tellus,* **24,** 199–215.

Lampe, B. & Holliger, K., 2003. Effects of fractal fluctuations in topographic relief, permittivity and conductivity on ground-penetrating radar antenna radiation, *Geophysics,* **68,** 1934–1944.

Le Stunff, Y., Grechka, V. & Tsvankin, I., 2001. Depth-domain velocity analysis in VTI media using surface P-wave data: is it feasible?, *Geophysics,* **66,** 897–903.

Lovell, M.A. & Odgen, P., 1984. Remote assessment of permeability/thermal diffusivity of consolidated clay sediments, Final Report EUR 9206 en, Commission of the European Communities, Nuclear Science and Technology, Luxembourg.

Lynn, H.B., 2004. The winds of change: Anisotropic rocks – their preferred direction of fluid flow and their asscociated seismic signatures – part 1, *Leading Edge,* **23,** 1156–1162.

Mondol, N.H., Bjørlykke, K., Jahren, J. & Høeg, K., 2007. Experimental mechanical compaction of clay mineral aggregates – changes in physical properties of mudstones during burial, *Marine Petroleum Geol.,* **24,** 289–311.

Muijs, R., Robertsson, J.O.A. & Holliger, K., 2004. Data-driven adaptive decomposition of multicomponent seabed recordings, *Geophysics,* **69,** 1329–1337.

Muijs, R., Robertsson, J.O.A. & Holliger, K., 2007. Data-driven adaptive decomposition of multicomponent seabed seismic recordings: application to shallow-water data from the North Sea, *Geophysics,* **72,** V133–V142.

Odom, R.I., Park, M., Mercer, J.A., Crosson, R.S. & Paik, P., 1996. Effects of transverse isotropy on modes and mode coupling in shallow water, *J. Acoust. soc. Am.,* **100,** 2079–2092.

Orszag, S.A., 1972. Comparison of pseudospectral and spectral approximation, *Stud. Appl. Math.,* **51,** 253–259.

Postma, G.W., 1955. Wave propagation in a stratified medium, *Geophysics,* **20,** 780–806.

Rotondo, K., 2004. Transport and deposition of fluid mud event layers along the Western Louisiana Inner Shelf, *Master's thesis,* Louisiana State University.

Sams, M.S., 1995. Attenuation and anisotropy: the effect of extra fine layering, *Geophysics,* **60,** 1646–1655.

Schalkwijk, K.M., Wapenaar, C.P.A. & Verschuur, D.J., 2003. Adaptive decomposition of multicomponent ocean-bottom seismic data into downgoing and upgoing P and S waves, *Geophysics,* **68,** 1091–1102.

Schneider, W.A. & Backus, M.M., 1964. Ocean-bottom seismic measurements off the California coast, *J. geophys. Res.,* **69,** 1135–1143.

Schoenberg, M. & Muir, F., 1989. A calculus for finely layered anisotropic media, *Geophysics,* **54,** 581–589.

Shepard, F.P., 1954. Nomenclature based on sand-silt-clay ratios, *J. Sedim. Petrol.,* **24,** 151–158.

Sheriff, R. & Geldart, L.P., 1995. *Exploration Seismology,* 2nd edn. Cambridge University Press, Cambridge.

Sidler, R. & Carcione, J.M., 2007. Wave reflection at an anelastic anisotropic ocean bottom, *Geophysics,* **72,** SM139–SM146.

Sidler, R., Carcione, J.M. & Holliger, K., 2008. On the evaluation of the plane-wave reflection coefficient, *Geophys. J. Int.,* **175,** 94–102.

Spencer, J.W.J., 1981. Stress relaxations at low frequencies in fluid-saturated rocks: attenuation and modulus dispersion, *J. geophys. Res.,* **86,** 1803–1812.

Stewart, R.R., Gaiser, J.E., Brown, R.J. & Lawton, D.C., 2002. Converted-wave seismic exploration: methods, *Geophysics,* **67,** 1348–1363.

Stewart, R.R., Gaiser, J.E., Brown, R.J. & Lawton, D.C., 2003. Converted-wave seismic exploration: applications, *Geophysics,* **68,** 40–57.

Stoll, R.D., 1989. *Sediment Acoustics,* Springer, Berlin.

Terwindt, J.H.J., Breusers, H.N.C. & Svasek, J.N., 1968. Experimantal investigation on the erosion-sensitivity of sand-clay lamination, *Sedimentology,* **11,** 105–114.

Tessmer, E., Kessler, D., Kosloff, D. & Behle, A., 1992. Multi-domain Chebyshev-Fourier method for the solution of the equations of motion of dynamic elasticity, *J.Compuat. Phys.,* **100,** 355–363.

Thomsen, L., 1986. Weak elastic anisotropy, *Geophysics,* **51,** 1954–1966.

Thomsen, L. & Dellinger, J., 2003. On shear-wave triplication in transversely isotropic media, *J. appl. Geophys.,* **54,** 289–296.

Tsvankin, I., 2005. *Seismic Signatures and Analysis of Reflection Data in Anisotropic Media.* 2nd edn, Elsevier, Amsterdam.

Tsvankin, I. & Thomsen, L., 1994. Nonhyperbolic reflection moveout in anisotropic media, *Geophysics,* **59,** 1290–1304.

Turcotte, D.L., 1997. *Fractals and Chaos in Geology and Geophysics.* 2nd edn, Cambridge University Press, Cambridge.

Ulrych, T.J., 1999. The whiteness hypothesis: Reflectivity, inversion, chaos, and Enders, *Geophysics,* **64,** 1512–1523.

Vega-Ruiz, D.S., 2003. Intrinsic and stress-induced velocity anisotropy in unconsolidated sands, *PhD thesis*, Stanford University.

Vernik, L. & Liu, X., 1997. Velocity anisotropy in shales: a petrophysical study, *Geophysics,* **62,** 521–532.

von Kármán, T., 1948. Progress in the statistical theory of turbulence, *J. Maritime Res.,* **7,** 252–264.

Wang, Y., Singh, S.C. & Barton, P.J., 2002. Separation of P- and SV-wavefields from multi-component seismic date in the τ–π domain, *Geophys. J. Int.,* **151,** 663–672.

Wang, Z., 2002. Seismic anisotropy in sedimentary rocks, part 2: Laboratory data, *Geophysics,* **67,** 1423–1440.

Zhou, B. & Greenhalgh, S., 2004. On the computation of elastic wave group velocities for a general anisotropic medium, *J. geophys. Eng.,* **1,** 205–215.